

# Optimizing stellarators for turbulent transport

H.E. Mynick<sup>1</sup>, N.Pomphrey<sup>1</sup>, and P. Xanthopoulos<sup>2</sup>

<sup>1</sup>*Plasma Physics Laboratory, Princeton University, Princeton, NJ*

<sup>2</sup>*Max-Planck-Institut für Plasmaphysik, Teilinstitut Greifswald, Greifswald, Germany*

Up to now, the term “transport-optimized” stellarators has meant optimized to minimize neoclassical transport, while the task of also mitigating turbulent transport, usually the dominant transport channel in such designs, has not been addressed, due to the complexity of plasma turbulence in stellarators. Here, we demonstrate that stellarators can also be designed to mitigate their turbulent transport, by making use of two powerful numerical tools not available until recently, namely gyrokinetic codes valid for 3D nonlinear simulations, and stellarator optimization codes. Two initial proof-of-principle configurations are obtained, reducing the level of ion temperature gradient turbulent transport from the NCSX baseline design by a factor of 2–2.5.

PACS #s: 52.55.Hc, 52.65.Tt, 52.35.Ra

Transport due to plasma turbulence has been a major challenge for magnetic confinement since the inception of the fusion program in the 1950s. Starting in the 1980s, a number of approaches to neoclassical-transport-optimized stellarators were discovered[1–5], in which the neoclassical (nc) transport could be reduced to below the level of turbulent or “anomalous” transport over most of the plasma column, making stellarator confinement comparable to that achievable in tokamaks. In recent years, two powerful numerical tools have been developed, which also make mitigating turbulent transport in stellarators a realistic possibility, namely configuration optimization codes such as Stellopt[6], and gyrokinetic (gk) codes valid for 3D configurations, such as the GENE/GIST code package[7, 8]. In this paper, we make use of these two new tools to demonstrate that new stellarator configurations with appreciably diminished turbulent transport levels can be evolved from stellarators designed without this turbulent-transport-optimization, raising the prospect of a new class of stellarators with greatly improved overall confinement.

Stellopt seeks to minimize a cost function  $C^2(\mathbf{z}) = \sum_i w_i^2 C_i^2(\mathbf{z})$  in the “shape space”  $\mathbf{z} \equiv \{z_j\}$  specifying a stellarator design, where the  $C_i^2$  are the contributions from any physics or engineering criteria the user wishes to apply, and the  $w_i$  are adjustable weights. (For the fixed-boundary equilibria we compute here, the  $z_j$  are the Fourier amplitudes specifying the boundary shape of the design. One could equally well take free-boundary equilibria, with the  $z_j$  the currents in the coil set.) For the turbulent contribution  $C_t^2$ , one could ideally take  $C_t = \langle Q_{gk} \rangle$ , the surface- or volume- averaged heat flux  $Q_{gk}$  from nonlinear GENE runs, but this would be far too computationally expensive, since many hundreds of individual configurations are evaluated in a typical optimizer run, and a nonlinear gk parallel simulation for a single flux tube for the present application requires on the order of 100 CPU-days. To surmount this obstacle, we instead employ a “proxy function”  $Q_{prox}$  in  $C_t^2$  to stand in place of  $Q_{gk}$ , a fairly simple function of key input geometric quantities, based on theory and on the geometry dependences of  $Q_{gk}$  found in GENE studies on

a family of nc-optimized stellarators.[9]  $Q_{prox}$  need not give a highly accurate prediction of what the gk result will be (though of course the more accurate the better) – it need only capture enough of the physics to guide the optimizer toward configurations which GENE will subsequently confirm has reduced  $Q_{gk}$ . Moreover, by examining the means by which Stellopt contrives to improve  $Q_{prox}$  and  $Q_{gk}$ , one may learn methods for deforming the stellarator shape to achieve the turbulent stabilization which are geometrically possible, whose discovery without the optimizer would be extremely difficult.

For  $Q_{prox}$ , we begin with an expression for the ion radial heat flux

$Q_i = -\chi n_0 g^{xx} dT_i/dx$ , with radial coordinate  $x \equiv (2\psi_t/B_a)^{1/2}$ ,  $2\pi\psi_t$  the toroidal flux,  $B_a$  the magnetic field strength  $B$  at the plasma edge (where  $x = a$ ), and  $g^{xx} \equiv |\nabla x|^2$  the  $xx$  component of the metric tensor. We use the quasilinear expression for the ion conductivity,  $\chi = \sum_{\mathbf{k}} D_{\mathbf{k}}$ , with

$$D_{\mathbf{k}} = (\omega_{*i} L_n)^2 \langle |\frac{e\phi_{\mathbf{k}}}{T_i}|^2 \rangle \gamma_{\mathbf{k}} / \omega_{\mathbf{k}}^2 \simeq c_D \gamma_{\mathbf{k}} / k_x^2. \quad (1)$$

Here,  $\omega_{*i} \equiv -(ck_y T_i / eB) \kappa_n$  is the diamagnetic frequency, with inverse density scale-length  $\kappa_n \equiv L_n^{-1} \equiv -\partial_x \ln n_0$  and  $k_y \equiv \mathbf{k} \cdot \hat{y}$  the wavevector component in the binormal direction  $\hat{y} \equiv \hat{b} \times \hat{x}$ , with  $\hat{x}$  and  $\hat{b}$  unit vectors in the directions normal to a flux surface and along the magnetic field. The final form is obtained using a simple mixing-length argument for the mean-square potential fluctuation amplitude  $\langle |\phi_{\mathbf{k}}|^2 \rangle$ , with  $c_D$  a multiplicative constant, determined below.

As in Ref. 9, for simplicity we consider only ion temperature gradient (ITG) turbulence[10] with adiabatic electrons. As found there, two geometric quantities central to determining the form and amplitude of the turbulence are the “radial curvature”  $\kappa_{\perp 1} \equiv \mathbf{e}_x \cdot \boldsymbol{\kappa}$ , with vector curvature  $\boldsymbol{\kappa}$  and  $\mathbf{e}_x$  the covariant basis vector for  $x$ ,[8] and the local shear  $s_l \equiv \partial_{\theta}(g^{xy}/g^{xx})$ , with  $\theta$  the poloidal azimuth in flux coordinates, which parametrizes distance along a field line. An approximate ITG dispersion equation is

$$0 \simeq \frac{1}{\tau} + \frac{\omega_{*i}(1 + \eta_i)\omega_{di}}{\omega^2} + \frac{k_{\parallel}^2 v_i^2 \omega_{*i}(1 + \eta_i)}{\omega^3}, \quad (2)$$

with  $\omega_{di} = -\omega_{*i}\kappa_1/\kappa_n$  the ion drift frequency,  $\eta_i \equiv \kappa_T/\kappa_n$ , and  $\kappa_T \equiv -\partial_x \ln T_i$ . The first term on the right side is the adiabatic electron contribution, the second term gives the ITG “toroidal branch”, and the third term gives the “slab branch”. If that 3rd term is neglected, Eq.(2) is quadratic in  $\omega$ , giving  $\omega \equiv \pm i\gamma_{\mathbf{k}} \simeq \pm \omega_{*i}[\tau(1 + \eta_i)\kappa_1/\kappa_n]^{1/2}$ , becoming unstable for  $\kappa_1 < 0$  (“bad curvature”). This expression has a critical pressure gradient  $\kappa_{cr} = 0$ , which becomes nonzero for a more complete dispersion equation, *e.g.*, from including the 3rd term in Eq.(2). Here, we include  $\kappa_{cr}$  simply as a parameter, by making the replacement  $(1 + \eta_i) \equiv \kappa_p/\kappa_n \rightarrow (\kappa_p - \kappa_{cr})/\kappa_n$ . Then one has

$$\gamma_{\mathbf{k}} \simeq (\omega_{*i}/\kappa_n)|\tau\kappa_1(\kappa_p - \kappa_{cr})|^{1/2}H(\kappa_p - \kappa_{cr})H(-\kappa_1), \quad (3)$$

with  $H(\kappa)$  the Heavyside function. Retaining the 3rd term in Eq.(2), and making the replacement  $k_{\parallel} \rightarrow -(i/qR)\partial_{\theta}$  (with  $R$  the major radius and  $q$  the safety factor) yields a Schrödinger equation, which localizes the mode in  $\theta$  to wells in the effective potential  $V_{ef}(\theta)$ , proportional to the first two terms in Eq.(2).[9]

We model  $k_x^{-2}$  on the intuition that  $s_l$  plays a role similar to that played by flow shear,[9] stabilizing the mode and diminishing its radial extent from the “mesoscale” ( $k_x^{-1} \sim \sqrt{L_p\rho_i}$ ) to a microscale ( $k_x^{-1} \sim \rho_i$ ) when the  $E \times B$  shearing frequency  $\omega_E$  becomes comparable to the inverse correlation time  $\tau_E^{-1}$  for fluctuations in the absence of  $E \times B$  flow[11]:

$$k_x^{-2}(\omega_E, s_l) \simeq \rho_i^2 + \rho_i L_p / [1 + (\tau_E \omega_E)^2 + \langle (\tau_s s_l)^2 \rangle_{\Delta\theta}]. \quad (4)$$

Here,  $\rho_i$  is the ion gyroradius,  $L_p \equiv \kappa_p^{-1}$ ,  $\tau_E, \tau_s$  are constants set below, and  $\langle \dots \rangle_{\Delta\theta}$  is an average along a field line weighted by a gaussian of width  $\Delta\theta$ , a simple means of giving  $k_x^{-2}$  the nonlocal character more rigorously imposed by actually solving the mode equation noted above along  $\mathbf{B}$ .  $Q_{prox}$  is thus determined by Eqs.(1),(3), and (4), which have 5 as yet undetermined constants,  $\kappa_{cr}, \tau_E, \tau_s, \Delta\theta$ , and  $c_D$ . Here, we neglect the flow-shear contribution (we set  $\tau_E = 0$ ), and fix the remaining 4 by using simulated annealing[12] to make a best fit of  $Q_{prox}$  with the  $Q_{gk}$  from the results of GENE simulations on the family of 3 flux tubes in each of 4 toroidal configurations studied in Ref. 9, giving values 0.053, 1.12, 0.207, and 0.959, respectively. A comparison of  $Q_{prox}$  (solid) and  $Q_{gk}$  (dashed) along one field line of each of these 4 configurations is given in Fig. 1. For all flux tubes simulated,  $Q_{prox}$  represents reasonably well the form of  $Q_{gk}$  along  $\mathbf{B}$ , and also gives the approximate magnitude in each case but for 2 of the 3 tubes simulated for W7X (Wendelstein VII-X)[13], where it is too small by a factor of about 3, indicating that some further physics is to be found to improve the present  $Q_{prox}$ . The predictive reliability of  $C_t^2$  is somewhat better than that indicated in Fig. 1, since it uses the surface average ( $Q_{prox}$ ) of  $Q_{prox}$ , and the local disparities in  $(Q_{prox} - Q_{gk})$  tend to cancel.

In Fig. 2 – Fig. 4 we show the results of two Stellopt runs using this  $Q_{prox}$ . The Levenberg-Marquardt

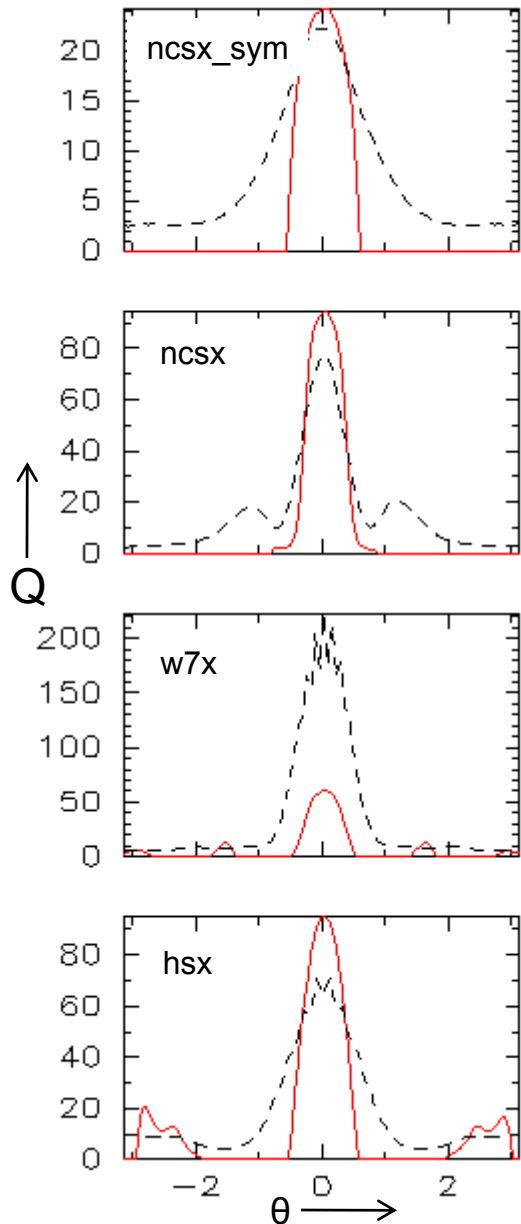


FIG. 1: (Color online) Comparison of  $Q_{prox}$  (red solid) with  $Q_{gk}$  (black dashed) for one flux tube of each of the 4 toroidal configurations studied in Ref. 9.

optimization scheme[14] Stellopt uses runs in successive “generations” of equilibria, here each with 54 members (one for each direction of shape space  $\mathbf{z}$ ), to determine the direction in  $\mathbf{z}$ -space to move next. For both cases, Stellopt begins with configuration LI383, which formed the baseline configuration for NCSX (National Compact Stellarator Experiment)[15], at  $\beta = 4.2\%$ .  $w_t$  is made large enough to make  $C_t^2$  dominate  $C^2$  for the first several generations. Constraints are also applied to main-

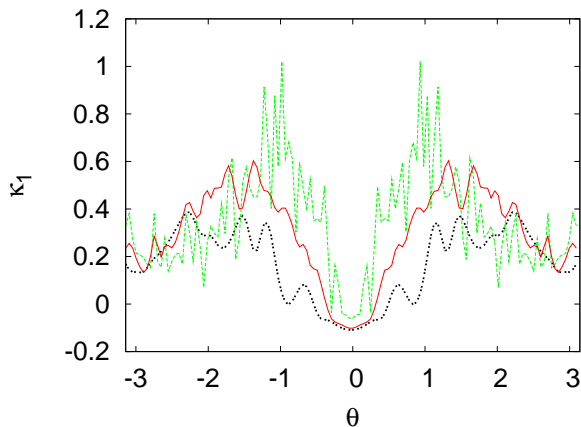


FIG. 2: (Color online) Comparison of radial curvature  $\kappa_1(\theta)$  for 1 poloidal transit for NCSX (heavy dashed black), QA\_35q (dashed green) and QA\_40n (solid red).

tain the plasma  $\beta$ , aspect ratio, and  $RB_t$  (= major radius  $\times$  toroidal field), but the configurations are otherwise unconstrained. After several generations, a sample equilibrium is chosen from each run, before the configurations become less interesting from a practical standpoint (for example, their rotational transform dropping excessively). We select a sample configuration “QA\_35q” from generation 4 of the first run, and “QA\_40n” from generation 7 of the second.  $C_t$  is 2 orders of magnitude below that of NCSX for QA\_35q, and about 1 order of magnitude for QA\_40n. The reason why is shown in Fig. 2, which compares radial curvature  $\kappa_1(\theta)$  for 1 poloidal transit for for NCSX (dashed black) with those for QA\_35q (dashed green) and QA\_40n (solid red). For both new configurations, one sees that Stellopt has found a means of boosting  $\kappa_1$  so that it has bad curvature ( $\kappa_1 < 0$ ) in a much narrower region than NCSX and worse curvature than NCSX only where  $\kappa_1 > 0$  for both configurations. While QA\_40n has a  $\kappa_1$  which is somewhat more oscillatory than for NCSX, and more so for QA\_35q, both have smooth, converged VMEC equilibria. In Fig. 3 we show the boundaries of NCSX (dashed black) and QA\_40n (solid red) for cross sections at 4 values of toroidal azimuth  $\zeta$ . The boundaries for QA\_35q are similar to those of QA\_40n.

While  $C_t$  has fallen orders of magnitude from that of NCSX, the decisive test of whether the new configurations truly have reduced transport is from nonlinear GENE runs. This comparison is given in Fig. 4, showing the line-averaged  $Q_{gk}$  for NCSX (dashed black), QA\_35q (dashed green) and QA\_40n (solid red) versus time. One sees that both indeed have  $Q_{gk}$  substantially diminished from that for NCSX, by a factor of about 2.5 for QA\_35q and about 2 for QA\_40n. The reduction is not as large as indicated by  $Q_{prox}$ , but the proxy is clearly adequate to guide Stellopt in the direction needed to reduce the turbulent transport. The achieved reduction is quite appreciable, comparable to the reduction achieved in tokamaks

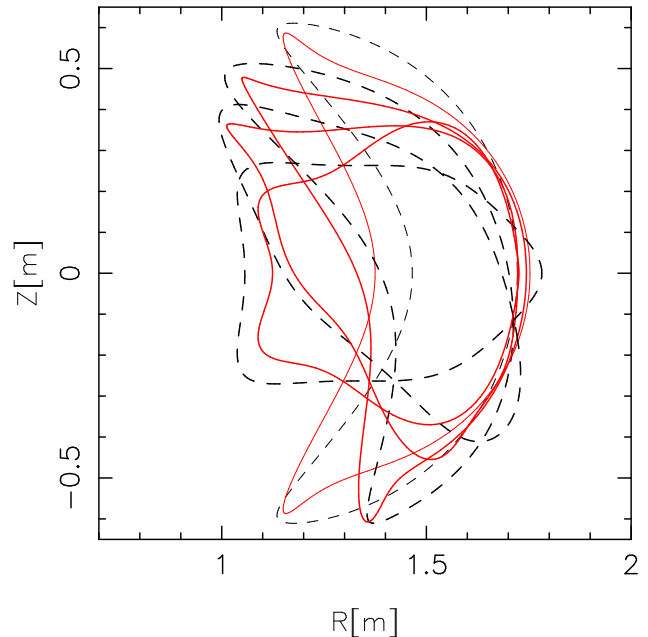


FIG. 3: (Color online) Comparison of boundary shapes of NCSX (dashed black) and QA\_35q (solid red) at values of  $N\zeta$  (= number of field periods  $\times$  toroidal angle) =  $0, \pm\pi/2, \pi$ .

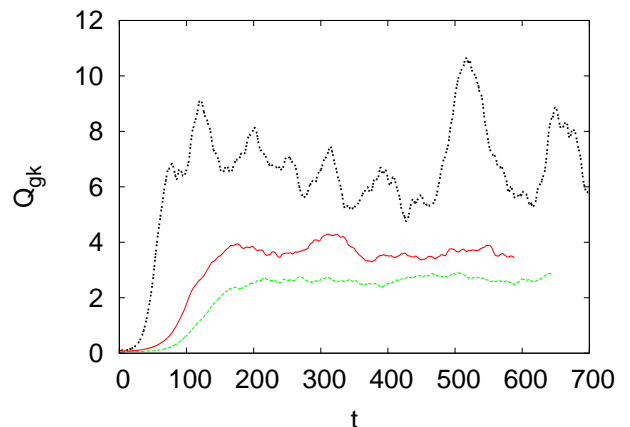


FIG. 4: (Color online) Comparison of line-averaged heat flux  $Q_{gk}$  versus time for NCSX (heavy dashed black), QA\_35q (dashed green), and QA\_40n (solid red) from nonlinear GENE runs. QA\_35q and QA\_40n achieve reductions in turbulent transport over that in NCSX by factors of about 2.5 and 2, resp.

in going from L- to H-mode.

While QA\_35q fares somewhat better than QA\_40n in its  $Q_{prox}$  and  $Q_{gk}$ , it does worse in its nc transport level, as assessed by its “ $1/\nu$ ” nc value  $Q_{nc} \sim \epsilon_{ef}^{3/2}/\nu$ , with  $\epsilon_{ef}$  the configuration’s “effective ripple strength”, and  $\nu$  the thermal collision frequency. QA\_35q has  $\epsilon_{ef}^{3/2}$  about 30 times that of NCSX. However, the high degree of nc optimization present in NCSX makes its predicted ripple transport smaller than that of its estimated turbu-

lent transport by about the same amount,[16] so that nc transport is still not dominant for this configuration. In contrast, QA.40n actually has *better*  $Q_{nc}$  than NCSX, with  $\epsilon_{ef}^{3/2}$  about 0.6 times that of NCSX.

QA.35q and QA.40n were arrived at using almost the same Stellopt parameters, the main difference being the selection of different representations for the boundary in producing the equilibria. This small difference set Stellopt on two similar but different courses through shape space, owing largely to the highly structured topography of  $C^2(\mathbf{z})$ . These two systems provide the first “proof-of-principle” that substantial turbulence mitigation can indeed be achieved by 3D shaping using this approach. However, in evolving them, Stellopt did not apply various constraints to the configurations to make them fully satisfactory. For example, while mostly ballooning stable, as is LI383, QA.35q and QA.40n are kink unstable, and their rotational transforms are smaller than that of LI383 by factors of about 2.7 and 1.6, respectively. As found from earlier experience in finding attractive candidate designs, including for example LI383 and the N3ARE design derived from it,[17, 18] finding configurations satisfying multiple constraints can often be achieved, but the trajectory through shape space is a multi-staged process, requiring human assessment and adjustment.

Many further possibilities exist for making use of this general approach to turbulent transport mitigation. The reduction Stellopt achieved in QA.35q and QA.40n principally made use of the  $\kappa_1$ -dependence of  $Q_{prox}$ , finding a

means of deforming NCSX to restrict the domain of bad curvature, and thereby alleviate the ITG instability. In a similar way, one may seek other configurations which reduce transport by using the  $s_l$ -dependence in  $Q_{prox}$ . Also, as noted, the present  $Q_{prox}$  can be improved as a model for ITG transport, and one may expect further improvements would accrue as more of the significant physics in  $Q_{gk}$  is captured by  $Q_{prox}$ . Further, the present restriction to ITG turbulence was taken only for simplicity – any modes which gk codes such as GENE can compute (*e.g.*, trapped-electron or electron temperature-gradient modes) can be addressed by this method, developing a modified  $Q_{prox}$  guided by theory and by gk studies of  $Q_{gk}$ . Moreover, it will also be of interest to use starting designs other than NCSX, to see what different means of achieving transport reduction Stellopt finds as the initial configuration is varied. For example, each of the nc-transport-optimized designs studied in Ref. 9, and perhaps tokamaks, would provide an edifying testbed for this approach. Work addressing these avenues has been initiated.

### Acknowledgment

The authors are grateful to A. Boozer, L. Maingi, G. Rewoldt, and E. Valeo for valuable discussions. This work supported by U.S.Department of Energy Contract No.DE-AC02-09CH11466.

- 
- [1] H.E. Mynick, T.K.Chu, A.H.Boozer, *Phys. Rev. Letters* **48**, 322 (1982).
  - [2] A.H. Boozer, *Phys.Fluids* **26** 496 (1983).
  - [3] J. Nührenberg, R. Zille, *Phys. Lett. A* **129**, 113 (1988).
  - [4] J. Nührenberg, W. Lotz, and S. Gori, in *Theory of Fusion Plasmas*, E. Sindoni, F. Tryon and J. Vaclavik eds., SIF, Bologna, (1994).
  - [5] P.R. Garabedian, *Phys. Plasmas* **3**, 2483 (1996).
  - [6] A. Reiman, G. Fu, S. Hirshman, L. Ku, *et al.*, *Plasma Phys. Control. Fusion* **41** B273 (1999).
  - [7] F. Jenko, W. Dorland, M. Kotschenreuther, B.N. Rogers, *Phys. Plasmas* **7**, 1904 (2000).
  - [8] P. Xanthopoulos, W. A. Cooper, F. Jenko, Yu. Turkin, A. Runov J. Geiger, *Phys. Plasmas* **16**, 082303 (2009).
  - [9] H.E. Mynick, P. Xanthopoulos and A.H. Boozer, *Phys.Plasmas* **16** 110702 (2009).
  - [10] F. Romanelli, *Physics of Fluids B* **1**, 1018 (1989).
  - [11] J. Garcí'a, K. Yamazaki, J. Dies, J. Izquierdo, *Plasma physics and controlled fusion* **48**, p15-27, (2006).
  - [12] Wm. H. Press, *et al.*, *Numerical Recipes in Fortran 77*, (Cambridge University Press, 1996), p.436ff.
  - [13] G. Grieger, W. Lotz, P. Merkel, *et al.*, *Phys. Fluids -B* **4**, 2081 (1992).
  - [14] Wm. H. Press, *et al.*, *Numerical Recipes in Fortran 77*, p.676ff.
  - [15] G.H. Neilson, M.C. Zarnstorff, J.F. Lyon, the NCSX Team, *Journal of Plasma and Fusion Research* **78**, 214-219 (2002).
  - [16] D.R. Mikkelsen, H. Maassberg, M.C. Zarnstorff, C.D. Beidler, W.A. Houlberg, W. Kernbichler, H. Mynick, D.A. Spong, P. Strand, V. Tribaldos, *Fusion Science and Technology* **51** 166 (2007).
  - [17] L.P. Ku, P. Garabedian, *Fusion Science and Technology*, **50** 207 (2006).
  - [18] H.E. Mynick, A.H. Boozer, L.-P. Ku, *Phys. Plasmas* **13**, 064505 (2006).